Supporting Information

UiO-66-NH_2 Fabrics: Role of Trifluoroacetic Acid as Modulator on MOF Uniform Coating on Electrospun Nanofibers and Efficient Decontamination of Chemical Warfare Agent Simulants

Xiuling Zhang[1,2,3⊥], Yaxin Sun[1,2,3⊥], Yuanfeng Liu[1,2,3], Zhenyu Zhai[1,2,3], Shiquan Guo[1,2,3], Lichong Peng[1,2,3], Yue Qin[1,2,3], Congju Li[1,2,3*]

1 School of Energy and Environmental Engineering, University of Science and Technology Beijing, Beijing 100083, China;
2 Beijing Key Laboratory of Resource-oriented Treatment of Industrial pollutants, Beijing 100083, China；
3 Energy Conservation and Environmental Protection Engineering Research Center in Universities of Beijing, Beijing 100083, China.

Corresponding author: congjuli@126.com

UiO-66-NH_2 powder: 0.233 g of Zirconium tetrachloride ($ZrCl_4$,) and 0.181 g of BDC-NH_2 were mixed with 0.16 mL of 12 M HCl and 10 mL DMF solvent. After that, benzoic acid (0.244 g) was added to the above solution by ultrasonication until the precursors were completely dissolved. Subsequently, the solution was transferred into 50 mL Teflon-lined autoclave for 48 h at 120 ˚C. Finally, the sample was washed with DMF and ethanol for three times, respectively and dried under vacuum oven (24 h, 60 □). The sample was denoted by UiO-66-NH_2 powder without TFA.

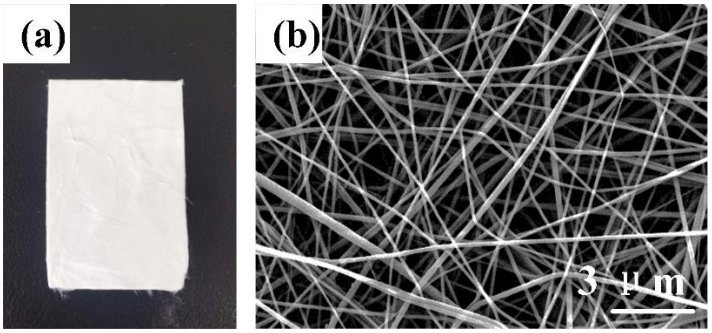

Figure S1. (a) Optical image and (b) SEM image of bulk PAN nanofiber membrane.

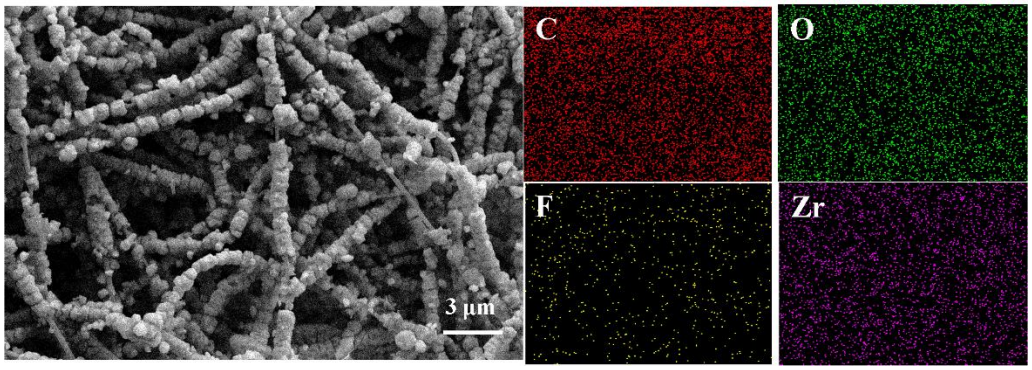

Figure S2. The Element mapping images of C, O, F and Zr in UiO-66-NH_2@PAN-2h.

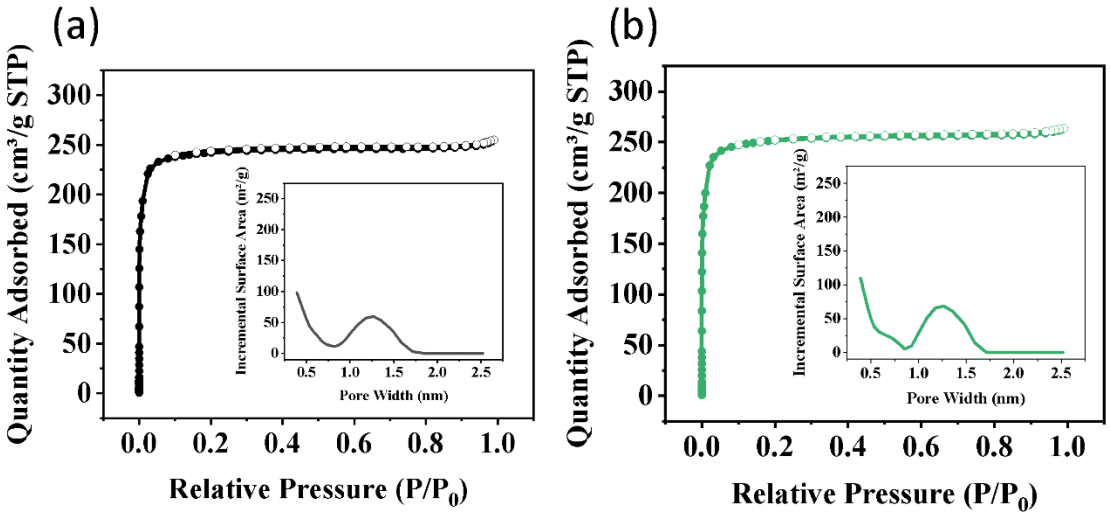

Figure S3. N_2 sorption isotherms of UiO-66-NH_2@PAN-1h (a) and UiO-66-NH_2@PAN-4h (b) the distribution of pore size of inset images.

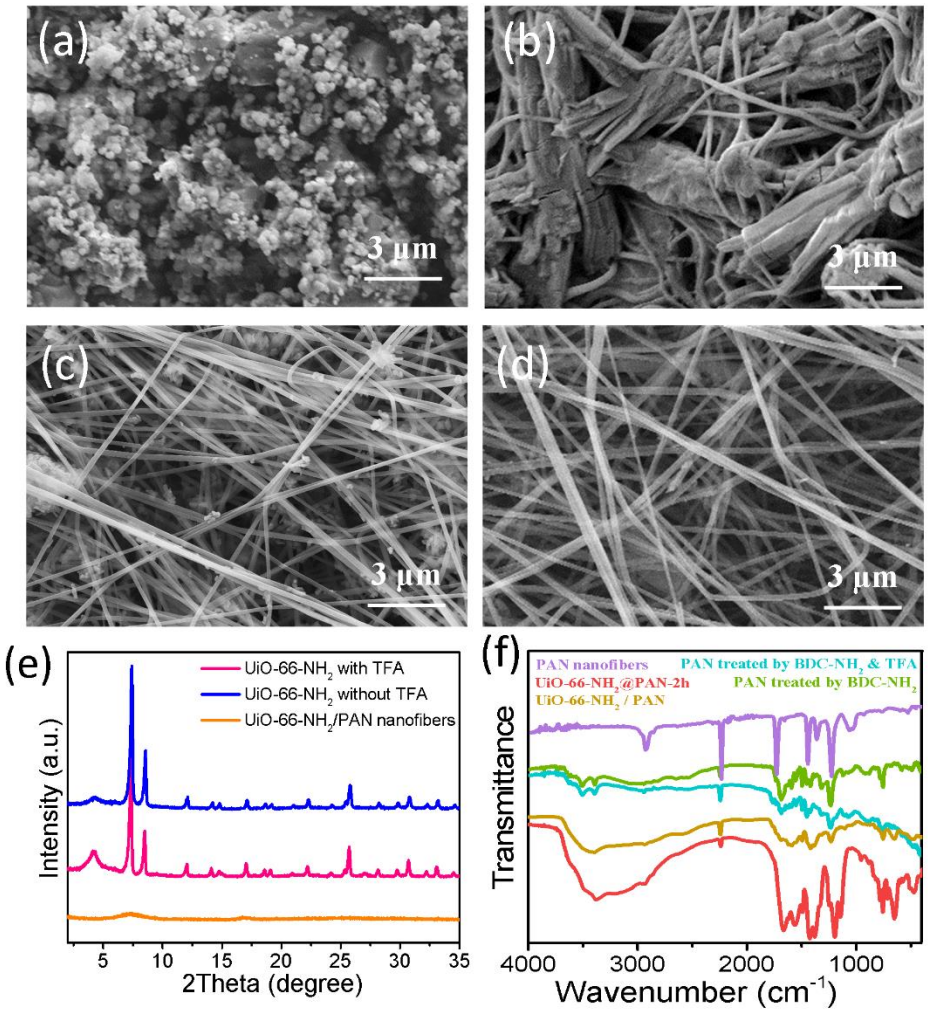

Figure S4. SEM images of UiO-66-NH_2 powder (a); SEM images of UiO-66-NH_2/PAN nanofibers (b), PAN nanofibers only treated by BDC-NH_2 (c), PAN nanofibers treated by BDC-NH_2 and TFA for 2 h (d); XRD patterns (e), FTIR spectrum of different samples (f).

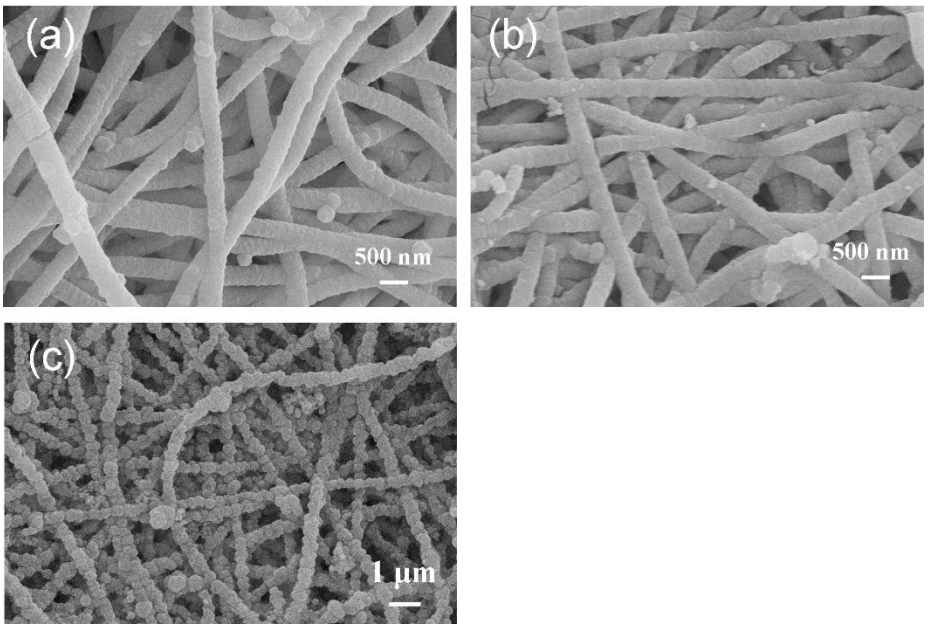

Figure S5. SEM images indicating the changes of PAN fibers surface. After reaction of 10 min (a), 20 min (b) and 30 min (c).

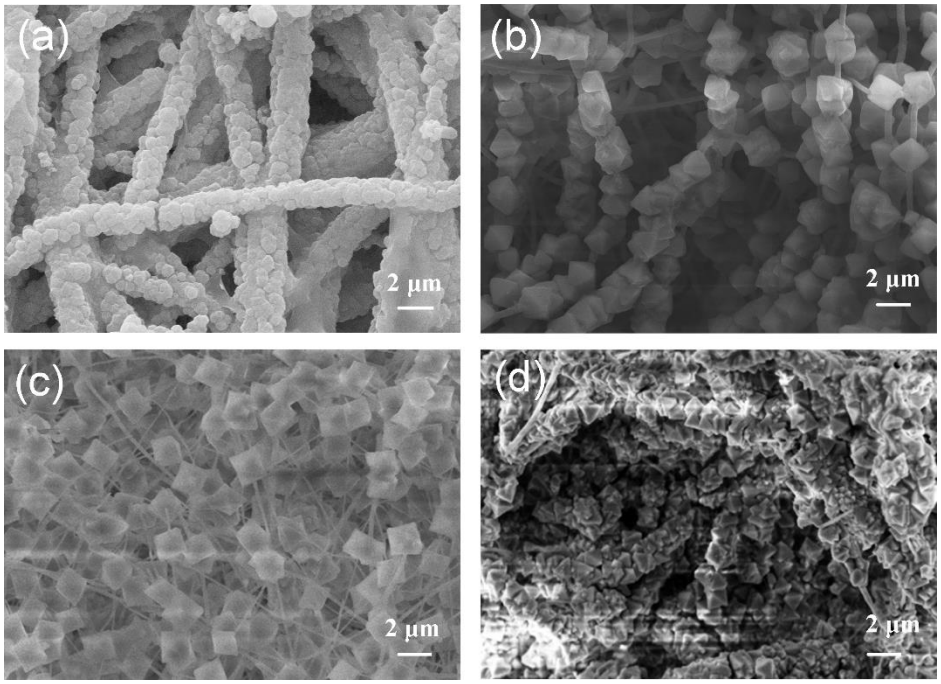

Figure S6. The SEM images of UiO-66-NH_2@TPU (a), MOF-808@PAN (b), UiO-66-NO_2@PAN (c) and UiO-66-NO_2@PVDF (d).

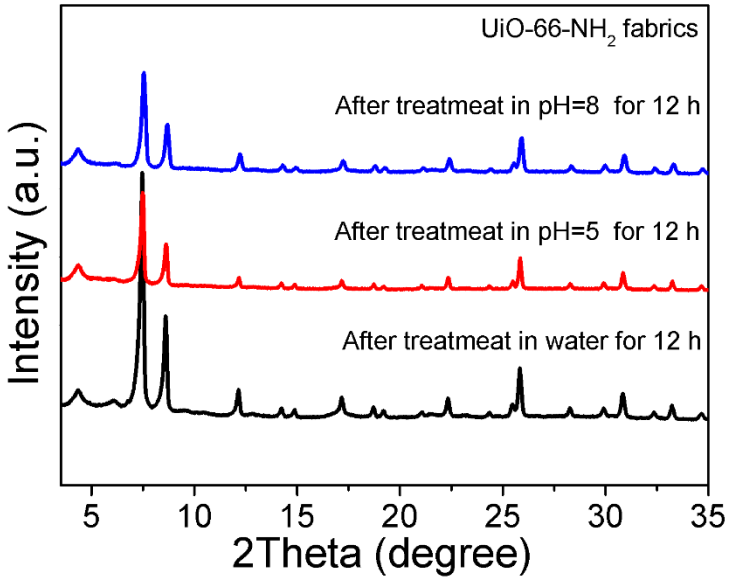

Figure S7. The PXRD of UiO-66-NH_2@PAN-2h after treated with different aqueous solution.

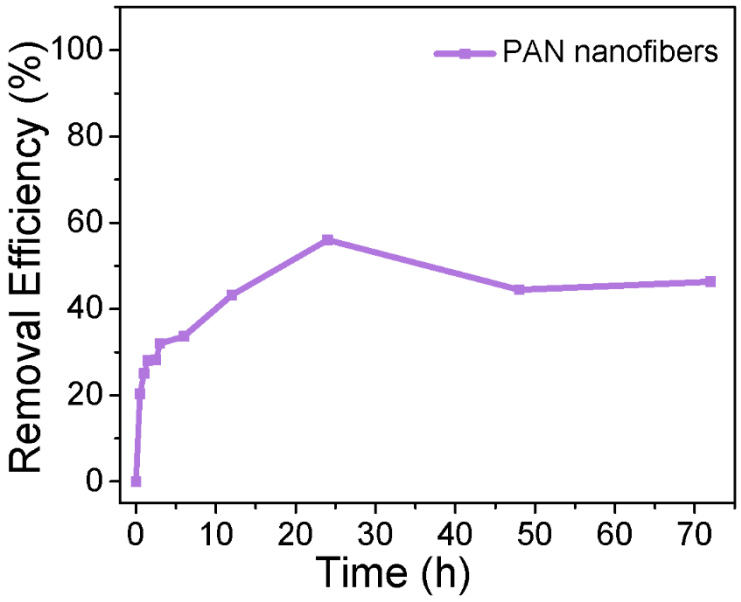

Figure S8. The profiles of removal efficiency for PAN.

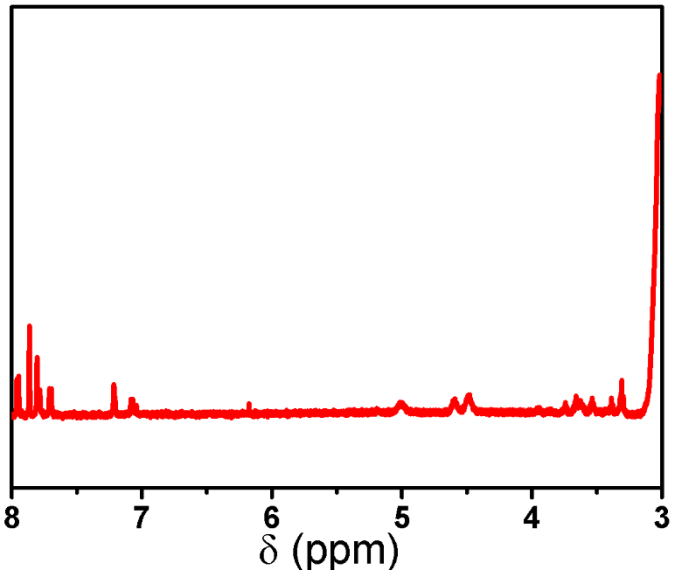

Figure S9. ^{1}H NMR of UiO-66-NH_2@PAN-2h exposed to CEES for 72 h and digested in H_2SO_4/DMSO.

Table S1. FTIR modes of PAN and UiO-66-NH_2@PAN composite materials.

Wavenumber (cm^{-1})	Mode
2935	C-H stretching vibration
2240	-CN group stretching vibration
1454	CH_2 bending vibration
680, 764	Zr−O
1569, 1430, 1389	COO^-
3488, 3380, 1626	$-NH_2$

Table S2. The comparison of four samples of BET.

Sample	$S_{BET}(m^2/g)$	Pore volume (cm^3/g)	Average pore size (nm)
UiO-66-NH_2@PAN-1h	816.4	0.395	1.933
UiO-66-NH_2@PAN-2h	958.7	0.459	1.916
UiO-66-NH_2@PAN-4h	849.6	0.407	1.921

Table S3. The mass change after washing in different pH.

	Before cleaning m_1 (mg)	After cleaning12h m_2 (mg)	Mass loss (%)
Deionized water	10.92	10.03	8.15
NaOH (aq) pH=8.0	13.22	12.54	5.14
HCl (aq) pH=5.0	11.85	11.03	6.92